Simultaneous depth determination of multiple objects by focus analysis in digital holography

Mark L. Tachiki,[1] Masahide Itoh,[1] and Toyohiko Yatagai[1,2,*]

[1] *Institute of Applied Physics, University of Tsukuba, Tennodai 1-1-1, Tsukuba, Ibaraki 305-8573, Japan*

[2] *Center for Optical Research and Education, Utsunomiya University, Yoto 7-1-2, Utsunomiya, Tochigi 321-8585, Japan*

[*] *Corresponding author: yatagai@cc.utsunomiya-u.ac.jp*

Focus analysis techniques from computer vision are applied to digital holography to determine the depth (range) of multiple objects and their surfaces from a single hologram capture. With this method the depths of objects can be determined from a single hologram capture without the need for manual focusing, and without prior information on object location. Variance and Laplacian of Gaussian are analyzed as focus measures, and techniques are proposed for focus plane determination from the focus measure curves. The algorithm is described in detail and demonstrated through simulation and optical experiment.

OCIS codes: (090.0090) Holography; (100.0100) Image processing; (110.0110) Imaging systems; (120.0120) Instrumentation, measurement and metrology; (150.0150) Machine vision.

1. Introduction

Focus analysis has been used extensively in the field of computer vision to locate objects from a single viewing position [1, 2]. The typical process in these systems is (a) to locate the outlines of objects using some edge detection algorithm and (b) to determine the distance (or range, depth) to each object through focus analysis. The image may be divided into smaller *cells* [3], for which the focus measure is optimized. In these methods object locations and shapes do not always need to be predicted, but rather each cell can be considered as a distinct and separate object or partial object. Usually, the peak of the focus measure in the depth axis gives the focus position.

Focus analysis has also been investigated in holography. In a method described by Ma [4], a hologram was recorded conventionally on a plate, developed, then scanned at high resolution. Spatial variance is used effectively as a simple focus measure to measure shape. Although the paper describes the method as digital holography, this is digital holography in the original sense of scanning a hologram developed from an exposure on a plate or film. Thelen demonstrated a method for measuring object surface shape from focus analysis in conventional holography by recording optical reconstruction images by CCD then analyzing the slices by computer [5]. This

method also requires the labor of developing the hologram, as well as optical setup for reconstruction. With fully-automated digital holography utilizing a CCD camera, obtaining hologram reconstructions of a relatively large object with low noise and high resolution is much more difficult. In particular, speckle noise becomes a problem when the hologram dimensions are limited.

Other methods of evaluating focus in digital holography have been developed. The use of self-entropy as a focus measure in digital holography has been investigated [6], but this method is used to analyze the focus of entire images of a single object, not on multiple objects or specific object features. Similarly, integrated amplitude modulus has been proposed as a focus measure [7], but it has only been proven with whole objects as well. Liebling introduced the use of Fresnelets to calculate object location, but this also has the limitation that the entire object must be identified prior to calculation [8]. Ferraro investigated a method to track focus for objects in motion [9], in which the initial focus adjustment must be done manually. Yu described a method of iterative reconstruction that uses irradiance as a simple focus measure across the entire image [10]. This method is less likely to work for images with subtle shades of gray.

Various methods for shape measurement exist in holography. However, these methods are only capable of finding the shape of continuous object surfaces, not their depths. Other interferometric methods exist that can be used to determine object depth, but these require some mechanical adjustment and multiple image captures,

so they may not be suitable for measuring moving objects.

In this work a system for determining the depth of objects using focus analysis in digital holography is proposed and developed. This might be thought of as a photographic auto-focus system which is capable of focusing on multiple objects in a single scene *after* the photograph is taken. Original solutions are proposed and demonstrated for problems inherent in depth by focus algorithms such as determining the depth of object areas with no high contrast features, and filtering of areas of the reconstruction image with no objects at all. To our knowledge, this type of system has not been implemented before in digital holography.

The key advantage of this system is that independent objects in space can be located in a single hologram capture. This makes it valuable in measurements of objects that may be moving in space (such as objects in a fluid). This method is capable of determining objects depths to moderate resolution without requiring long calculation times as in deconvolution [11].

2. Algorithm development

In this section the proposed measurement algorithm, particular difficulties encountered, and proposed solutions are explained in detail.

Here is a brief overview of the algorithm.

1. Image slices are reconstructed from the hologram at succcessive depths.
2. Each slice is divided into equally sized subimages called *cells*.

3. The focus measure is calculated for each cell in each slice.
4. For each cell, the variation in the focus measure and irradiance over depth is analyzed.
5. The depth of the object or object portion (or lack of object) in each cell is determined.

The variation of focus measure over depth is called the *focus curve*. Note that the units are generally arbitrary, since the focus measure may not always have a direct physical significance.

2.A. Reconstruction algorithm

First, multiple slices at incremental planes parallel to the hologram plane centered on the optical axis are reconstructed from the digital hologram. The reconstruction range and slice spacing must be determined by the user. In this work, the hologram plane is several centimeters from the object, so hologram reconstruction is performed using the Fresnel transformation [12]

$$f_r(x_r, y_r) = \frac{j}{\lambda}\frac{e^{jkd}}{d}\iint_{\infty} f_h(x_h, y_h)\exp\left\{-\frac{ik}{2d}\left[(x_r - x_h)^2 + (y_r - y_h)^2\right]\right\} dx_h\, dy_h \quad (1)$$

where $f_r(x_r, y_r)$ is the reconstructed slice at distance d from the hologram $f_h(x_h, y_h)$, k is the propagation constant, and λ is the wavelength of the light. Note that the lateral position and size of each cell in reconstruction space varies depending on the reconstruction distance, growing larger and drifting farther from the optic axis as

distance increases. After reconstruction of each slice, median filtering is performed. Median filtering is effective in removing noise without disrupting edges, as long as the filter size is kept smaller than object feature sizes.

2.B. Focus analysis algorithm

Various focus measures have been demonstrated in computer vision. Almost all of them are based on edge detection algorithms, which can usually be divided into two broad categories: spatial-based and non-spatial-based. Non-spatial based edge detectors are generally simpler and do not consider the positions of each pixel intensity. An example is the variance focus measure, in which the variance of pixel intensity is calculated.

Spatial-based focus measurement can be divided further into two categories: first derivative and second derivative. First derivative edge detectors measure the amount of *activity* in the cell in one axis, where activity is the sum of the absolute value of the local derivative at each location in the cell. Examples include the Sobel, Prewitt, and Canny [13] detectors. Second derivative edge detectors are similar to first-derivative edge detectors except that they calculate the second derivative. Examples include the Laplacian of Gaussian (LoG) detector [14]. Second derivative edge detectors are known to be sensitive to noise, so it is important to use adequate filtering when they are used.

In this work, one example of a spatial-based focus measure and one example of a

non-spatial-based focus measure are analyzed.

In the shape by focus work of Ma [4], variance was used as a focus measure. This was effective in that work and is implemented in this work as well. The variance focus measurement simply measures the variance in the irradiance of the pixels in the cell. The only adjustable parameter is the size of the cells.

The Laplacian of Gaussian (LoG) method is a second derivative edge detector that is widely used because it is sensitive to edges, and is omni-directional. Marr found evidence that human vision uses mechanisms similar to LoG to locate objects in a scene [15]. Nayar adapted the LoG method to be a focus measure for shape measurement and called it the modified sum Laplacian [3]. Rather than looking at zero-crossings of the LoG to locate edges, Nayar found that integrating the absolute value of the LoG result over the image area yielded an effective focus measure that had an approximately Gaussian focus curve in the depth axis. Here it is adapted for depth measurement.

The Laplacian operator (written ∇^2) is the multidimensional generalization of the 2nd derivative. In Cartesian coordinates it is given by

$$\nabla^2 f = \frac{d^2 f}{dx^2} + \frac{d^2 f}{dy^2} \tag{2}$$

Marr noted that when using the Laplacian as an edge detector, the image first needs to be filtered because the Laplacian is sensitive to noise. The ideal filter for this was determined to be the Gaussian, since it has minimal extent in both the spatial and

spatial-frequency domains. Thus, the result of filtering with a Gaussian filter then taking the Laplacian is

$$\begin{aligned} f_{filtered}(x,y) &= \nabla^2[G(x,y) * f_{image}(x,y)] \\ &= \nabla^2 G(x,y) * f_{image}(x,y) \end{aligned} \tag{3}$$

where $G(x,y)$ is the Gaussian filter given by

$$G(x,y) = \frac{1}{2}\pi\sigma^2 \exp\left(\frac{-(x^2+y^2)}{2\sigma^2}\right) \tag{4}$$

where σ is the radius where the filter center lobe amplitude falls to 1/e or roughly 61%. Thus, Gaussian filtering and the Laplacian operation can be performed at the same time by simply filtering the image by the *Laplacian of Gaussian* filter $\nabla^2 G$. Taking the Laplacian of the Gaussian filter gives

$$\nabla^2 G(x,y) = \frac{1}{\sigma^3(2\pi)^{\frac{1}{2}}}\left(1 - \frac{x^2+y^2}{\sigma^2}\right)\exp\left[\frac{-(x^2+y^2)}{2\sigma^2}\right] \tag{5}$$

The result of this filtering is a positive and negative peak on either side of an edge. In the modified sum Laplacian focus measure, Nayar takes the absolute value of the result and sums the pixel values in the cell. The same procedure is used in this work, but it is referred to as "LoG". The LoG focus measure has three parameters: (a) the cell size in pixels, (b) the filter size in pixels, and (c) σ, the extent of the Gaussian filter. The cell width in pixels should be no smaller than σ, and the filter size should be at least 1.8σ pixels to capture the filter shape to less than 0.05 of the center amplitude. There is no advantage to using a filter wider than 3.0σ pixels and

the computational load increases as well.

With either focus measure, the focus measure is calculated for each cell in each slice, and stored in an array for analysis.

2.C. Focus plane locationing

Finally, the focus measure and irradiance variation over depth are analyzed to locate the ideal focus plane for each cell.

For a cell with distinct edges, the ideal focus location is generally given by the peak of the focus curve. However, for cells in which a featureless object surface occupies the entire cell (which shall be called *flats*) the depth generally corresponds to the minimum of the focus curve. This is because the out-of-focus energy of nearby contrast features of the same object are minimal when those features are in focus. Furthermore, cells with no objects (which shall be called *blanks*) will have low focus measures but will still have positive and negative peaks in the focus curve, so the focus analysis algorithm must be able to ignore these cells to avoid cluttering the result with the locations of false objects.

These cells that have low focus measures (flats and blanks) shall be collectively called *voids*. It is found that cells with distinct object features tend to have relatively high focus measure values at all depths. This characteristic is used to determine if a cell is a void: if any part of the focus curve of a cell falls below an arbitrary *focus threshold* (for example, 1/4 of the median of cell focus measures for all slices) it is

judged to be a void.

An example of a focus curve for a flat void cell completely occupied by an object at 20 cm from the hologram is shown in Fig. 1. The hologram is computer-generated using an ideal object. For reference, the mean and median of the focus measures of all slices of all cells are also shown, along with an example focus threshold arbitrarily set to half of the median. For flat voids, the ideal focus depth is the depth of minimum focus measure, as shown in Fig. 1 at 20 cm. In this example, the focus measure falls below the focus threshold at some points, so the cell is judged to be a void.

However, for a blank void, the depth of minimum focus measure usually corresponds to the depth of the nearest object. Thus the focus curve for a blank void will be at a minimum when the nearest object is in focus. This is shown in Fig. 2, the focus curve for an empty cell with nearby objects. Evaluating such a blank void cell in the same manner as a flat void would lead to a mapping of false objects to what is actually empty space.

To discriminate between blank and flat voids, the median irradiance of the cell at the depth of minimum focus measure is compared to an arbitrary *irradiance threshold*. If the median irradiance is low, the cell is deemed a blank void, otherwise it is determined to be a flat void. It is important to consider the median irradiance of the cell instead of peak irradiance because a completely blank area with a few high irradiance noise pixels could easily cause a false decision. A typical threshold is 1/10 of the median irradiance of all slices of all cells.

If the cell is not deemed a void, it is called an *edge cell*, and its focus position is determined by locating a peak according to criteria described below. An example of a focus curve for an edge cell is shown in Fig. 3.

Note that the ideal thresholds for void determination and flat/blank differentiation vary, as they depend on the size and shape of the filter, the irradiance of objects in the cell and surrounding cells, the size of the cell, and the shape of the objects. The thresholds may need to be adjusted by the user manually based on these factors.

2.D. Peak qualification

In computer vision, the maximum of the focus curve normally corresponds to the ideal focus position. To help avoid false determinations in digital holography, the depth determination algorithm is refined. In holography the maximum of the focus curve may become suppressed if the dominant contrast feature is small in extent and located in an otherwise featureless cell surrounded by strong edges just outside the cell. The peak in the focus curve caused by the feature coming into focus may be offset by a sharp dip in the focus measure caused by the sudden reduction in defocused noise if the neighboring objects are at a comparable depth. The focus algorithm will fail to recognize this suppressed peak, as shown in Fig. 4.

To find peaks that are hidden in a trough of the focus curve, various false determinations were examined. It is observed that true peaks tend to be symmetrical, while false peaks will be more gradual with bumps along the slopes. For true peaks, the

relative height will be roughly the same value on each side of the peak, while for false peaks one side will have a relatively shallow trough. Taking advantage of this characteristic, instead of finding the absolute peak of the focus curve, the local peak with the largest height relative to the higher neighboring minimum is determined as shown in Fig. 5. This shall be called the *local peak height*. This is analogous to *prominence* in topography.

In addition to local peak height, it is observed that true peaks tend to be narrower than false peaks. The higher the contrast is at the edge, the narrower the peak will be. Figure 6 shows an example of this. To avoid selecting false peaks, peaks wider than a set threshold are ignored. The peak width is defined as the distance between the local minima on either side of a peak. This threshold can be adjusted depending on the characteristics of the edges in the image. If no peaks are narrower than the threshold, the cell is deemed a blank void.

2.E. Output data

The result of the measurement is a depth map showing the depth of the dominant object or partial object in each cell. For blank voids, the depth can be set to an arbitrary background depth. In addition, a composite reconstruction can be assembled using the depth data. This gives a complete in-focus image, as might be observed with an optical reconstruction of a conventional hologram by eye. However, all parts of the hologram can be brought into focus at once, unlike a single slice reconstruction.

3. Simulation

To demonstrate the algorithm in a controlled environment, the algorithm is run on computer generated holograms with and without noise added.

3.A. Reference hologram synthesis

For simulation purposes, reference holograms are created using computer-generated holography (CGH). A test object is created consisting of an array of shapes. Rectangles have edges parallel to the axes of the rectangular coordinate system which the focus analysis algorithm operates with. Circles have curved edges, with edges at all possible angles. Triangles provide straight edges that are not parallel with the coordinate system axes. Lettering is placed inside the shapes to test the effectiveness of the method on finer objects with limited spatial extent (thickness).

The object array consists of three rows, one for each shape type, and three columns with different object depths as shown in Fig. 7. The objects are separated by ample distance to avoid overlap of defocus energy near the positions of ideal focus, but close enough that some degree of resolution is needed to differentiate the objects.

To simulate the speckle effect, a second hologram is created with object height randomized across the surface at a microscopic level by randomizing the phase of each pixel uniformly over the interval 0 to 2π. The speckle effect can create noise with high spatial frequency and contrast away from the focus position causing false peak detections.

The computer generated holograms are stored with 64-bit floating precision. Calculation of reconstruction slices to 16 bits is found to give satisfactory precision. Reconstruction slices of 480×480 are approximately 450 kB in size. A median filter is applied to the reconstructed slices of size 3×3 for the variance method and 5×5 for the LoG method. The filter sizes were found by trial and error.

3.B. Depth measurement

For the hologram without speckle, the focus position could be located to within 2mm with both methods, with the exception of some outlier cells. For the variance method, the outliers make up about 7% of object cells, and are mainly due to false peak detection due to instability in the focus measure near the hologram. For the LoG method, outliers make up about 23% of object cells, with the same false detections as in the variance method but also including some due to the presence of high contrast object edges just beyond the cell boundaries of blank cells.

The depth measurement results for the hologram with speckle are shown in Figs. 8 and 9. The (a) figures emphasize the object surfaces, while the (b) figures show the depth map from an overhead view to emphasize object outlines. Both methods are able to correctly locate most object surfaces to within 5 mm in the case with speckle. The number of falsely detected edge cells increased to 23% for the variance method and 53% for the LoG method. From the overhead view the object outlines are clearly visible. The composite reconstructions are shown in Fig. 10.

Particularly with the LoG method, in areas with *weak* edges, i.e. edges of small spatial extent compared to the cell area, the peak in the focus curve at the object position is obscured by focus measure noise from stronger edges in neighboring cells. In these cases, the noise of the speckle combined with out-of-focus energy from nearby objects cause more disturbance than the relatively localized edges. The stronger object outlines are detected correctly, while the fainter lettering is obscured by the speckle noise. A 5×5 median filter is used in reconstruction which helps in locating many of the flat voids, but the filter also partially erases some of the lettering since the lettering is only 2-3 pixels thick. However, in general the algorithm is effective in locating the correct focus planes. Note that the user can choose a larger cell size to improve the chances that larger objects are focused properly.

The variance focus measure is more consistent in finding the depth of object surfaces. It is more robust at smaller cell sizes, and is more immune to noise that the LoG method. Measurement time is also much faster with the variance focus measure, since a convolution is required in the LoG method. In both algorithms measurement errors are more common with objects nearer to the hologram. This is perhaps due to the fact that the depth of field is more shallow, causing peaks to be skipped due to undersampling. This could be avoided by reducing slice spacing for slices closer to the hologram.

3.C. Computation time

The algorithm is implemented in Matlab (version 6.5.1 Rel 13) for ease of development, and run on a Celeron 1.7 GHz processor with 768 MB of RAM. To measure a range of 15 cm to 35 cm in 1 mm increments, 201 slices are required. Reconstruction from the hologram and storage of the 480×480 reconstructed slices in lossless 16-bit PNG format to hard disk takes approximately 360 seconds for 201 slices. Normalization of the slices takes 170 seconds. Focus measure calculation with 40×40 cells takes about 22 seconds for the variance method, and 107 seconds for the LoG method. Analysis of focus curves takes approximately 8 seconds, and generation of the composite image takes 150 seconds. Total time to generate the composite image and depth maps from a hologram takes 12-13 minutes. Note however that after reconstruction has been performed once and slices are stored on hard disk, focus analysis itself only takes 30 seconds for the variance method and 115 seconds for the LoG method.

Virtually no time optimization has been done on the algorithm at this point, so vast improvement is possible through simple algorithmic changes. For example, normalization of the slices (170 seconds) could be eliminated by estimating the maximum irradiance from a single slice with minimal loss of dynamic range. Generation of the composite image (150 seconds) could be performed almost instantly if the slices could be stored in RAM. Vast improvement in computation time is also possible by porting to a compiled programming language.

4. Measurement system analysis

The expected behavior and performance of the system is discussed.

4.A. Depth accuracy and depth of field

Depth of field is the maximum amount by which the focus plane can deviate from the ideal focus position and still be able to resolve to a defined resolution in the defocused image.

As with computer vision, depth of field in holography is proportional to the range to the object and inversely proportional to the numerical aperture (NA) of the measurement system, which in this work is given by

$$NA = \frac{\text{hologram radius}}{\sqrt{\text{hologram radius}^2 + \text{object distance}^2}}, \tag{6}$$

which for an object at 25 cm and a hologram of 480×480 pixels with pitch of 9.9 µm gives an NA of 0.026.

Figure 11 shows the reconstruction irradiance profiles in the z-axis from a computer-generated hologram with point sources located at 10, 20, and 40 cm from the hologram with a hologram area of 3.3×3.3 mm. The profiles show that the depth of field is deeper for objects farther from the hologram. For the Fresnel transform reconstruction method the reconstruction pixel size increases as distance from the hologram increases. In contrast to computer vision (or photography) in which the diameter of defocus spots are linearly proportional to the distance from the ideal focus plane, the

defocus spots grow exponentially moving towards the hologram.

With a shallow depth of field a more accurate depth measurement is possible, and it may be easier to filter out false peaks. However, with a deeper depth of field the focus curve could be interpolated from a few points on the curve as demonstrated by Nayar [3]. Also, finer slice spacing is necessary if the depth of field is shallow, making a deeper depth of field more attractive if computation time is an issue.

4.B. Comparison of computer vision and holography

Here some of the physical and algorithmic differences between computer vision and holography are considered.

Computer vision is based on geometric optics, or ray optics. This means that the behavior of light can be modeled to reasonable accuracy using the Law of Reflection, the Law of Refraction (Snell's Law), and the Thin Lens Equation. Out-of-focus images of point objects have a Gaussian distribution [3]. The irradiance of out-of-focus light will add linearly with overlapping light from neighboring objects.

In holography, where coherent light is used and diffraction is occurring, physical optics must be considered. In reconstructions of holograms, a defocused point source will yield an Airy disk pattern instead of a simple Gaussian distribution. Out-of-focus energy from objects can interfere with energy from other objects and cause strong ripples in the image, because the complex field amplitudes are summed. This causes strong noise in the focus curve.

Object illumination is also more difficult in holography. In computer vision, multiple incoherent light sources are usually present, and in general light scatters off objects more uniformly in all directions. A lens in front of the CCD with an aperture much larger than the CCD captures a relatively wide angle of light from the object and focuses it onto the CCD. In holography, coherent light is used, and the unfocused light from the light source is recorded directly by the CCD. If the light source for the object beam is a plane wave, then light will tend to reflect off the object according to the Law of Reflection. Thus, lighting in digital holography is not as uniform, and more powerful light sources must be used for objects with low reflectivity.

Noise is also more of a problem in holography, due to the speckle effect. Thus, algorithms must be more complex and sacrifice computing time to deal with the noise.

In general, applying focus analysis to digital holography requires addressing some additional obstacles, and expectations on algorithm speed and accuracy need to be weighed against the properties of the objects being measured. However, many of the difficulties of holography can be avoided in microscopy due to increased reconstruction resolution.

5. Optical experiment

An optical experiment is performed to evaluate the performance of the focus analysis algorithm.

5.A. Optical setup

A Michelson interferometer setup is used to to record the holograms in-line. In this configuration, the object is illuminated normal to its surface.

A 632.8nm Helium-Neon 5mW gas laser is used. The laser beam is collimated to a roughly 3 cm radius using a 20x (NA 0.40) objective lens and a convex imaging lens of focal length 15 cm. The beam is split by a 2 cm square polarizing beam splitter, and adjusted using two neutral-density (ND) filters.

To maximize usable reconstruction resolution, phase-shift digital holography is performed using piezo-electric transducer (PZT) is used to actuate the mirror in the reference beam path [16]. Although this means that multiple hologram captures are performed, note that the method could also be performed with one hologram with an off-axis setup, although the measurable angle is reduced in half.

The hologram is recorded using a JAI CV-M4+CL 2/3" monochrome progressive scan CCD camera with 1340×1020 6.45 µm square pixels at 10 bits of pixel depth, and digitized using a National Instruments 1428 PCI frame grabber.

Test objects are created for measurement with the same dimensions as in the simulation. The objects themselves are pieces of overhead projector film with printed lettering, laminated with metallic film.

As in simulation, median filters of 3×3 for the variance method and 5×5 for the LoG method were applied to the reconstructed slices.

5.B. Data and results

Depth maps for the measurement using variance and the LoG method are shown in Figs. 12 and 13. Composite reconstructions are shown in Fig. 14.

The measurement is made difficult by the presence of excess light due to internal reflections in the beam splitter. In addition, strong images caused by reflections from the overhead transparency film surface add unwanted noise to the images. False measurements occur in cells where the object does not reflect enough light into the camera and where false images are present. In particular, a great amount of noise is present in the areas between the objects, partly due to phase shift inaccuracy. This leads to false measurements of blank voids, clouding the depth maps.

Also, the objects used in the experiment have multiple reflective layers that cause false images to appear in the reconstructions. In most objects it is unlikely that such images would appear. Inaccuracy in the phase shift and minute mechanical shifts in the optical system during mirror adjustment also cause noise, and could be improved by automation of the mirror actuation.

Though many cells have incorrect depth determinations, cells without false images and excessive noise are clearly in focus. In the composite reconstruction image for the variance method the lettering on the shapes are at least partially readable for most of the objects. Using the variance focus measure, over half of the object cells are measured to within 1 cm of accuracy. With the LoG method, perhaps one fourth

of the cells are measured to this accuracy. As in simulations, with the LoG method sensitivity to noise become a problem, and over half of the cells have incorrect depth determinations. However, the general depth of the objects can be estimated to some degree from the depth map.

6. Conclusion

In this work the use of focus analysis in digital holography as a method for determining the depth of multiple objects was explored. This method provides a way of determining the depth of objects without prior knowledge of object location. The algorithm can locate objects which are not part of a larger continuous object from a single hologram, which has not been demonstrated previously in digital holography.

Unique solutions were proposed for analysis of focus measure curves. The focus analysis algorithm was developed and demonstrated in both simulation and actual optical measurement. In experiments the algorithm was effective in locating objects and their object depths to within 1 cm from a range of 20 to 30 cm, particularly in areas of the reconstruction that are free of excess noise and false images. The variance method performed more effectively as a focus measure than the Laplacian of Gaussian method, both in depth accuracy and number of false detections.

As observed in experiments, this method is limited by the amount of noise present in reconstruction, and the proximity of objects. In particular, objects in close proximy in the x-y plane with a large depth difference can be difficult to detect properly due

to out-of-focus energy. Also, when the ratio of object (feature) size to object (feature) spacing is high, focus detection can be difficult.

Assuming these conditions are avoided, this method could be useful in measuring the locations of particles in liquids or gases if the density is relatively low. This method could be particularly effective in microscopy, where the effect of speckle can be less if surface height variations are less than one wavelength. Some modification of the algorithm would be necessary to differentiate flat and blank voids for a transmission-type measurement, but the basic focus measure concepts remains the same. This method could also be useful as an automated reconstruction method (autofocus) in general 3-D imaging systems. Discrepancies between the measured depth of objects and the depth calculated from the hologram could point to imperfections in the optical system, i.e. alignment.

References

1. R. Jarvis, "Focus optimisation criteria for computer image processing," Microscope 24, 163–180 (1976).
2. E. Kroktov, "Focusing," International Journal of Computer Vision 1(3), 223–237 (October 1987).
3. S. K. Nayar and Y. Nakagawa, "Shape from focus," IEEE Transactions on Pattern Analysis and Machine Intelligence 16(8), 824–831 (August 1994).
4. L. Ma, H. Wang, Y. Li, and H. Jin, "Numerical reconstruction of digital holograms

for three-dimensional shape measurement," J. Opt. Soc. Am. A 6(4), 396–400 (April 2004).

5. A. Thelen, J. Bongartz, D. Giel, S. Frey, and P. Hering, "Iterative focus detection in hologram tomography," J. Opt. Soc. Am. A 22(6), 1176–1180 (June 2005).
6. J. Gillespie and R. King, "The use of self-entropy as a focus measure in digital holography," Pattern Recognition Letters 9(1), 19–25 (January 1989).
7. F. Dubois, C. Schockaert, N. Callens, and C. Yourassowsky, "Focus plane detection criteria in digital holography microscopy by amplitude analysis," œ14(13), 5895–5908 (June 2006).
8. M. Liebling and M. Unser, "Autofocus for digital fresnel holograms by use of a fresnelet-sparsity criterion," J. Opt. Soc. Am. A 21(12), 2424–2430 (December 2004).
9. P. Ferraro, G. Coppola, S. De Nicola, A. Finizio, and G. Pierattini, "Digital holographic microscope with automatic focus tracking by detecting sample displacement in real time," Opt. Lett. 28(14), 1257–1259 (July 2003).
10. L. Yu and L. Cai, "Iterative algorithm with a constraint condition for numerical reconstruction of a three-dimensional object from its hologram," J. Opt. Soc. Am. A 18(5), 1033–1045 (May 2001).
11. J. G. McNally, T. Karpova, J. Cooper, and J. A. Conchello, "Three-dimensional imaging by deconvolution microscopy," Methods 19, 373–385 (May 1999).

12. U. Schnars and W. Jüptner, "Direct recording of holograms by a ccd-target and numerical reconstruction," Appl. Opt. 33(2), 179–181 (January 1994).

13. J. Canny, "A computational approach to edge detection," IEEE Transactions on Pattern Analysis and Machine Intelligence 8(6), 679–698 (January 1986).

14. E. C. Hildreth, "Implementation of a theory of edge detection," Technical report, MIT Artificial Intelligence Lab Technical Report 579, Massachusetts Institute of Technology, 1980.

15. D. Marr and E. C. Hildreth, "Theory of edge detection," Proceedings of the Royal Society of London 207, 187–210 (1980).

16. I. Yamaguchi and T. Zhang, "Phase-shifting digital holography," Opt. Lett. 22(16), 1403–1405 (August 1997).

7. List of figure captions

Fig. 1. (COLOR ONLINE) Focus curve for a flat void cell.

Fig. 2. (COLOR ONLINE) Focus curve for a blank void cell.

Fig. 3. (COLOR ONLINE) Focus curve for an edge cell.

Fig. 4. Focus measure suppressed by surrounding flat void.

Fig. 5. (COLOR ONLINE) Calculation of local peak height.

Fig. 6. (COLOR ONLINE) Peak widths for true and false peaks.

Fig. 7. Object intensity distributions for test computer-generated hologram.

Fig. 8. (a) 3-D and (b) 2-D depth maps for measurement simulation using variance.

Fig. 9. (a) 3-D and (b) 2-D depth maps for measurement simulation using Laplacian of Gaussian.

Fig. 10. Composite reconstruction for measurement using (a) variance and (b) Laplacian of Gaussian.

Fig. 11. Defocus irradiance profiles in holography.

Fig. 12. (a) 3-D and (b) 2-D depth maps for the measurement using variance.

Fig. 13. (a) 3-D and (b) 2-D depth maps for the measurement using Laplacian of Gaussian.

Fig. 14. Composite reconstruction for the measurement.

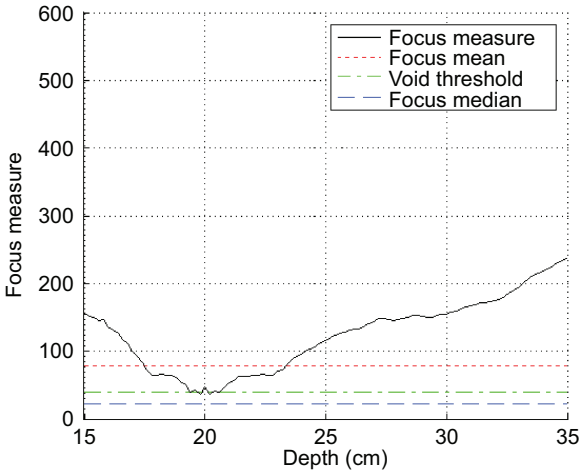

Fig. 1. (COLOR ONLINE) Focus curve for a flat void cell.

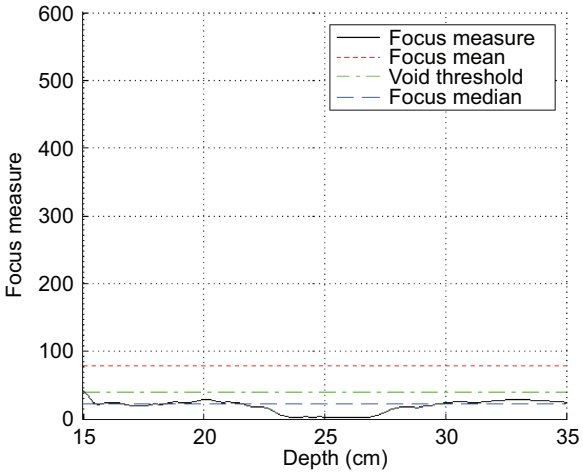

Fig. 2. (COLOR ONLINE) Focus curve for a blank void cell.

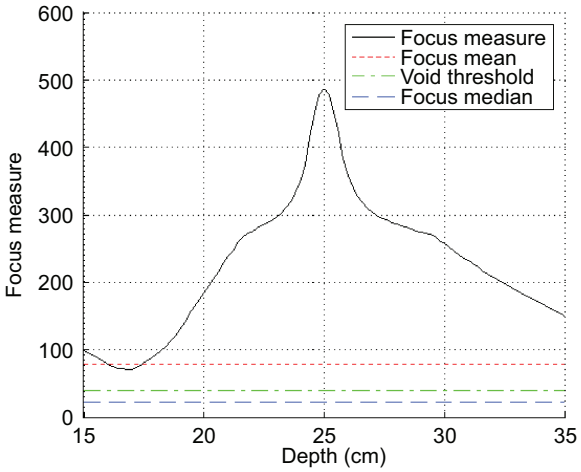

Fig. 3. (COLOR ONLINE) Focus curve for an edge cell.

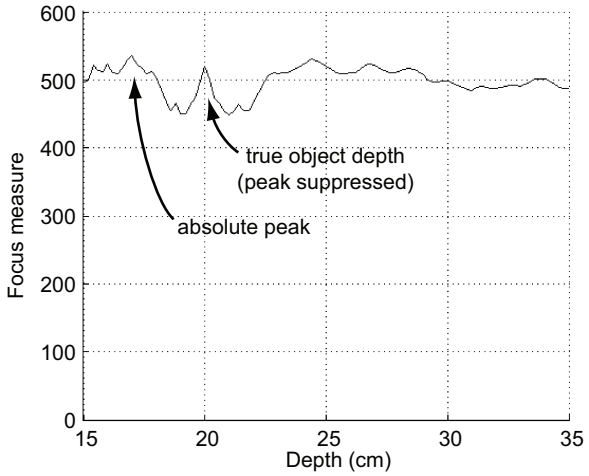

Fig. 4. Focus measure suppressed by surrounding flat void.

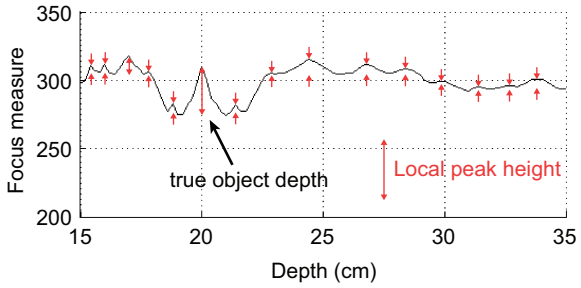

Fig. 5. (COLOR ONLINE) Calculation of local peak height.

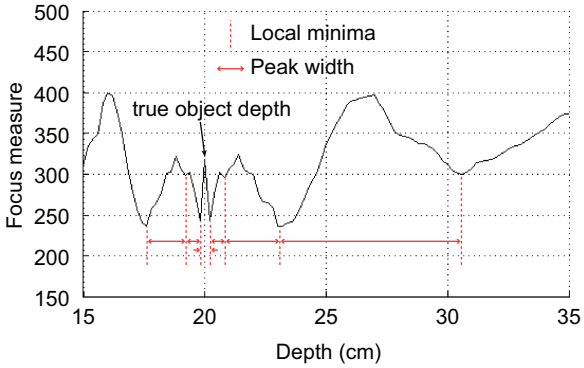

Fig. 6. (COLOR ONLINE) Peak widths for true and false peaks.

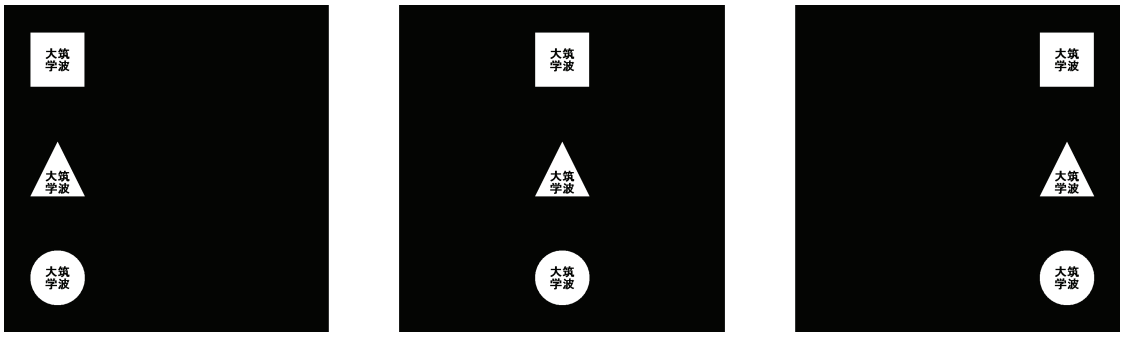

(a) 20 cm (b) 25 cm (c) 30 cm

Fig. 7. Object intensity distributions for test computer-generated hologram.

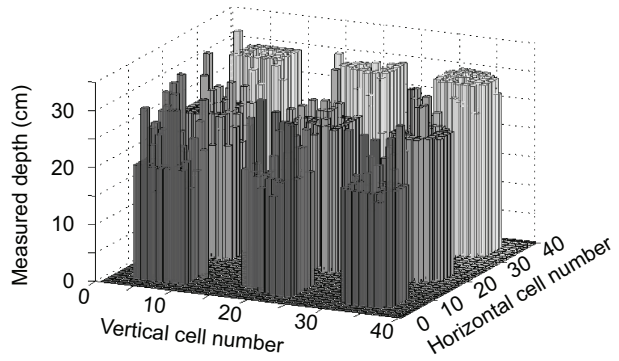

(a)

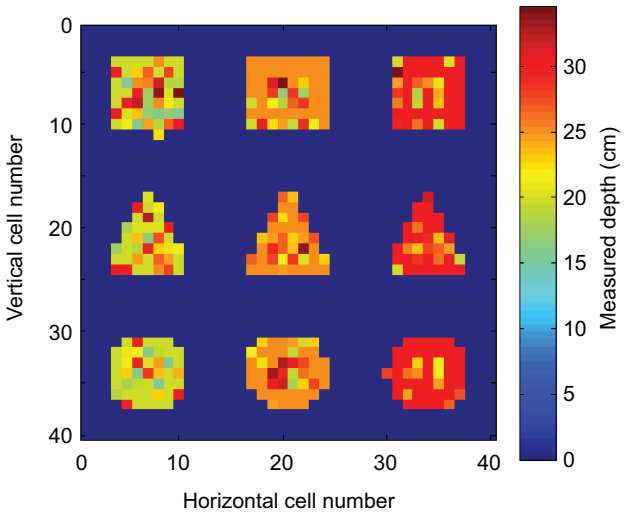

(b)

Fig. 8. (a) 3-D and (b) 2-D depth maps for measurement simulation using variance.

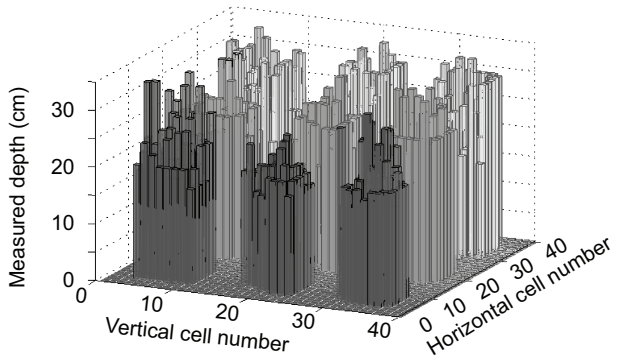

(a)

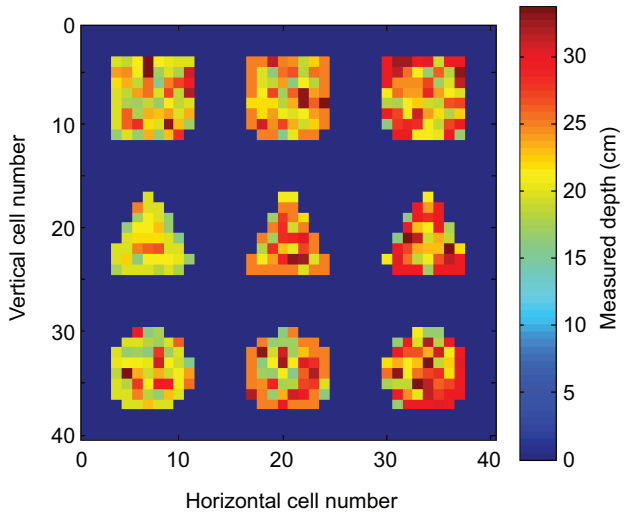

(b)

Fig. 9. (a) 3-D and (b) 2-D depth maps for measurement simulation using Laplacian of Gaussian.

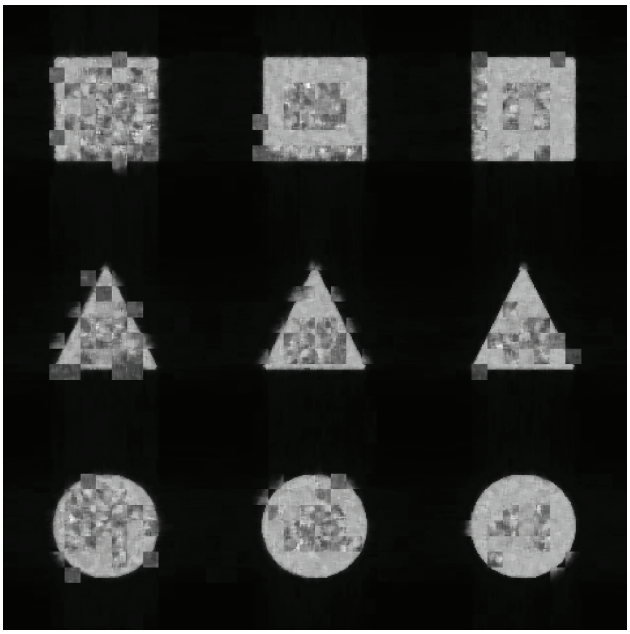

(a) variance

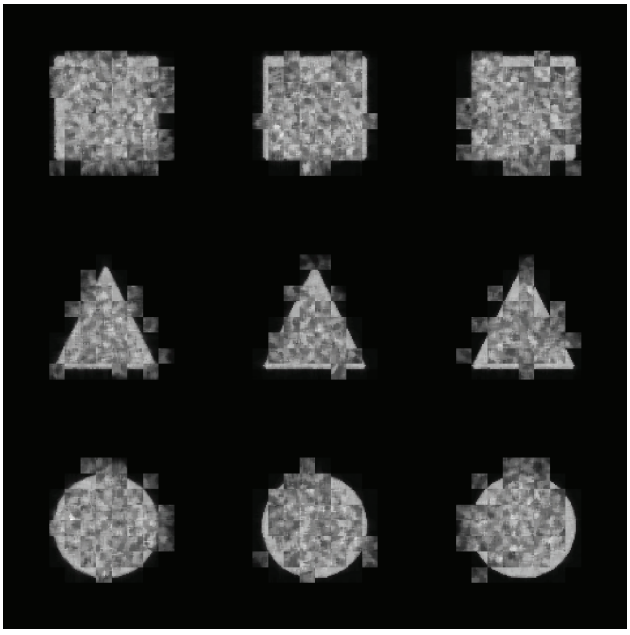

(b) Laplacian of Gaussian

Fig. 10. Composite reconstruction for measurement using (a) variance and (b) Laplacian of Gaussian.

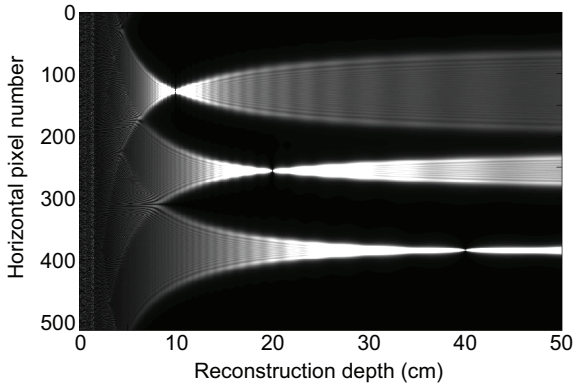

Fig. 11. Defocus irradiance profiles in holography.

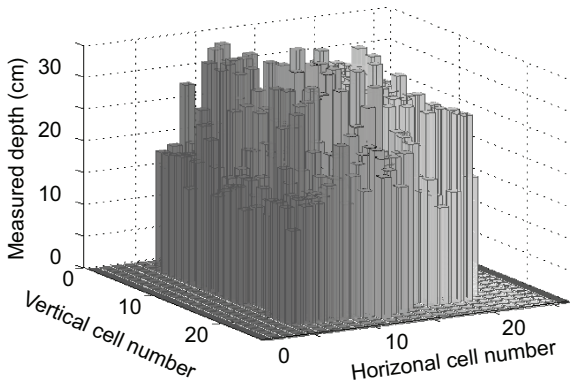

(a)

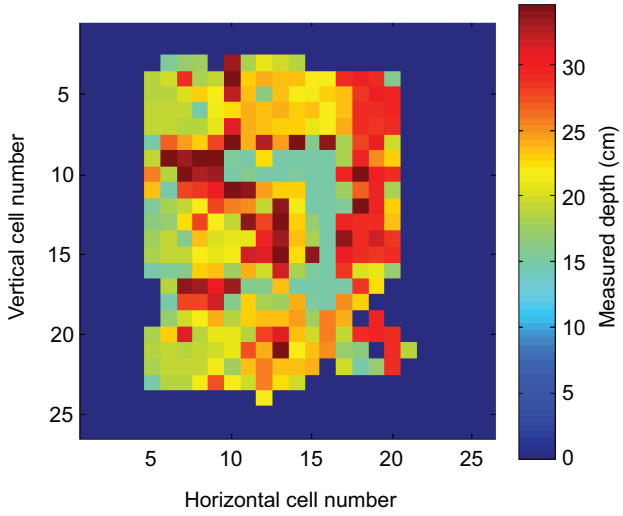

(b)

Fig. 12. (a) 3-D and (b) 2-D depth maps for the range measurement using variance.

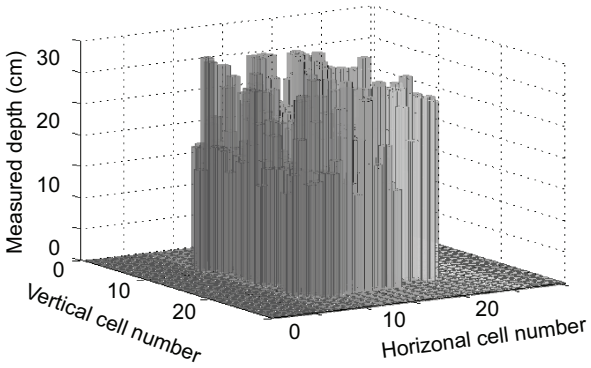

(a)

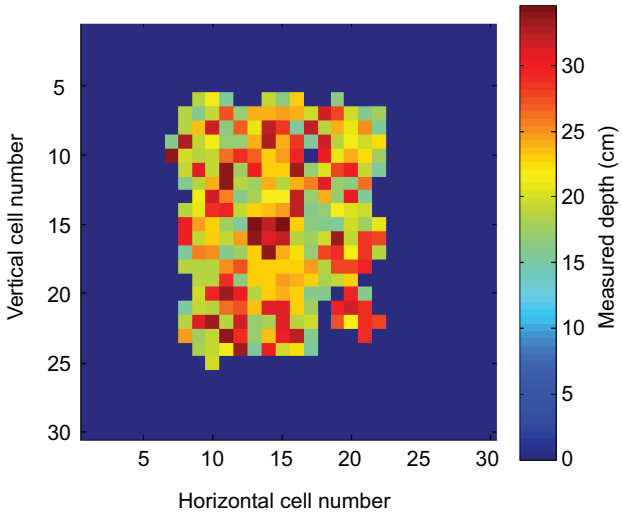

(b)

Fig. 13. (a) 3-D and (b) 2-D depth maps for the range measurement using Laplacian of Gaussian.

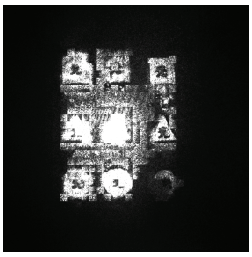

(a) variance

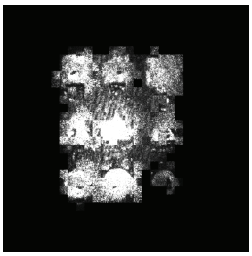

(b) Laplace of Gaussian

Fig. 14. Composite reconstruction for the range measurement.